Ultrasonics 96 (2019) 196–202

Contents lists available at ScienceDirect

Ultrasonics

journal homepage: www.elsevier.com/locate/ultras

Investigation of ultrasonic absorption in the MHz frequency range by silicon substrates with a built-in porous silicon layer

J. Lascaud, T. Defforge, G. Gautier, D. Certon*

GREMAN UMR 7347, Université de Tours, CNRS, INSA Centre Val de Loire, 16 rue Pierre et Marie Curie, 37071 Tours cedex 2, France

ARTICLE INFO

Keywords:
Porous silicon
Ultrasound transducers
Substrate
Attenuation

ABSTRACT

The present study is focused on the development and characterization of an innovative substrate to optimize the axial resolution of ultrasonic transducers on a silicon substrate that is dedicated to ultrasound imaging. The substrate must efficiently dampen wave propagation to avoid degradation of the axial resolution of ultrasound images. In this study, the proposed approach implements a silicon substrate with a built-in acoustic damping layer composed of porous silicon. Porous silicon layers with thicknesses of less than 100 μm and porosities varying from 27% to 62% were fabricated, and their substrate resonances were characterized. The experimental results obtained in the frequency range from 6 MHz to 10 MHz show that the substrate acoustic damping is controlled by adjusting the characteristics of the porous silicon layer; a significant damping of 70% is demonstrated with only 70 μm of porous silicon.

1. Introduction

The present study focused on the development and characterization of an innovative substrate to optimize the axial resolution of ultrasonic transducers on a silicon (Si) substrate that are dedicated to ultrasound imaging. Significant progress has been achieved in the field of ultrasound imaging since its first use for medical applications in the middle of the 20th century. Concomitant advances in ultrasound transducer technologies and the microelectronic industry have paved the way for new imaging modalities, such as real-time 3D imaging [1], intravascular imaging [2] and, more recently, wearable ultrasound patches [3,4]. These recent modalities have necessitated the development of more sophisticated systems that include electronic and ultrasonic transducer integration on the same chip. These chips have been supported by the development of new transducer technologies that are fabricated on a Si substrate, such as micromachined ultrasonic transducers, which are based on micrometric vibrating membranes [5,6]. These technologies are based on the same manufacturing processes as those used for microelectronics. Consequently, they enable 3D integration of the ultrasonic transducer and the front-end electronics required for the imaging system on the same chip. For this purpose, integrated electronic circuits are usually bonded to the rear side of the ultrasonic transducer substrate, and the electrical connections are transferred from the transducer side to the substrate rear side through the substrate [7].

The acoustic resonance of the substrate (the so-called thickness-mode resonances) is one of the drawbacks inherent to the technology of ultrasonic transducers on Si substrates. Indeed, a part of the ultrasonic wave produced by the transducer is transmitted to the supporting substrate. These substrate waves interfere with the transducer acoustic response and distort the impulse response [8]. Especially for imaging purposes, the thickness-mode resonance is responsible for an elongation of the impulse response, which degrades the axial resolution. Furthermore, parts of the substrate wave are radiated into the propagation medium, leading to imaging artefacts [9]. It is thus fundamentally necessary to dampen the substrate resonance to preserve image quality. To date, and to the best of our knowledge, no method compatible with the 3D integration of ultrasonic transducers can attenuate these substrate waves. Some authors have proposed gluing a millimetre-thick film on the opposite side of the transducer [10]. This film is composed of an attenuating material such as tungsten powder in an epoxy matrix. Nevertheless, the attenuating film avoids the 3D integration required for maintaining the ultrasound sensing function and the front-end electronics on the same chip. Another strategy to reduce the influence of wave propagation is by decreasing the thickness of the substrate [10]. The substrate thickness-mode resonance frequency is then increased and shifted outside the frequency range of interest. This second method allows for 3D electronic integration but does not avoid substrate wave propagation, which remains a potential artefact source for imaging.

* Corresponding author.
E-mail address: dominique.certon@univ-tours.fr (D. Certon).

https://doi.org/10.1016/j.ultras.2019.01.006
Received 14 September 2018; Received in revised form 23 January 2019; Accepted 26 January 2019
Available online 07 February 2019

Hereby, the substrate is based on a Si wafer with a built-in acoustic damping layer in porous silicon (PS) to reduce wave propagation in the substrate. PS is usually obtained by the electrochemical etching of a Si wafer in a hydrofluoric acid-based electrolyte [11]. This process is fully compatible with microelectronic processes and joint integration of a localized PS area; furthermore, the electronic components have already been proposed [12]. Then, the use of a PS layer to dampen the substrate waves is compatible with 3D integration of the ultrasonic transducer and the electronic components. The pore dimensions of the PS range from a few nanometres to tens of micrometres, and several layer structures can be achieved, as summarized in [13] (e.g., periodic, branched or random). The layer characteristics (i.e., thickness and porosity) are controlled by adjusting the etching conditions [14]. The porosity, defined as the ratio between the void volume and the Si volume, mainly depends on the hydrofluoric acid concentration of the electrolyte and the current density applied during electrochemical etching [15], while the layer thickness depends on the etching duration. It should be noted that PS formation by electrochemical etching is a top-down technique; therefore, although the Si layer thickness decreases, the total thickness of the Si/PS bilayer remains constant and equal to the initial thickness of the Si wafer. The opportunity to locally change the properties of the Si substrate has already attracted interest in numerous fields, such as optical systems (e.g., photonic crystals for sensing [16]) and acoustics (e.g., phononic crystals for filtering [17]), and the effect of the porosity on the PS bulk acoustic properties (e.g., the characteristic acoustic impedance and attenuation) has already been discussed in the literature [18–20]. For air-filled PS layers, the attenuation is proportional to the porosity, whereas the acoustic impedance is inversely proportional to the porosity, and varies from the Si characteristic acoustic impedance to the air characteristic acoustic impedance. In other words, a high porosity ($> 60\%$) is favourable to a significant attenuation, but its acoustic characteristic impedance ($<9 \times 10^5$ kg·s·m^{-2}) differs greatly from that of Si (19.7×10^5 kg·s·m^{-2}), leading to an important acoustic mismatch at the Si/PS interface (transmission coefficient < 0.6). Furthermore, from a technological point of view, the synthesis of a stable highly porous or thick PS layer (> 100 µm) is non-trivial. Indeed, the mechanical stress in this type of PS may result in the cracking and peeling of the porous layer or a millimetre curvature of the wafer [21]. Hence, the main challenge is to find a suitable trade-off between the thickness and the porosity of the PS layer to obtain significant acoustic damping (i.e., superior to the measurement uncertainties, which were estimated to be 16% in this work).

In this study, a series of Si substrate samples with built-in PS layers of different morphological characteristics were fabricated and characterized. A description of the fabrication method and the corresponding sample characteristics are provided in the first part of this article. The quality factor of the thickness-mode resonance was monitored to evaluate the changes in the acoustic damping of the substrate. Both the experimental protocol developed for this purpose and the theoretical model, which is based on transmission line theory, used to interpret the results are described in the first part of the article. In the second part of the article, the experimental and theoretical results are discussed and analysed. The phenomena responsible for the substrate resonance damping are discussed, and generalized rules for the design of thin damping layers are proposed.

2. Methodology

2.1. Sample fabrication

The PS layers were obtained by electrochemical etching in an electrolyte composed of 30 wt% hydrofluoric acid and 25 wt% acetic acid. This type of electrolyte was chosen to obtain porosity values between 30% and 60%. In this study, only mesoporous silicon obtained from highly doped Si and formed of nanometre-scale voids was investigated (see Fig. S1 in the supporting information) since highly doped Si is favourable to electronic integration (i.e., it is used as the bottom electrode for the ultrasonic transducers and to transfer the electrical contacts through the substrate). The PS layers were formed on a 133 cm^2 microelectronic standard and commercial Si wafer that are available from MEMC; 6-inch (1 0 0)-oriented p-type Si wafers have a thickness of 508 ± 15 µm and a resistivity of 20 mΩ·cm. The porosity was controlled by adjusting the current density from 10 mA/cm^2 to 50 mA/cm^2 and 80 mA/cm^2. The thicknesses of the PS layers were kept under 80 µm to preserve the mechanical stability of the PS layers. The etching durations were adjusted to obtain layer thicknesses of 80 µm (i.e., the maximum value) for each current density, and intermediate thicknesses of approximately 20 µm and 40 µm were arbitrarily chosen. For each sample, SEM cross-sectional observations were used to estimate the PS layer thickness (h_{PS}). The average porosity (Φ) was evaluated by gravimetry [22,23]. For this purpose, the silicon wafer mass (m_1) was measured before the PS etching. Freshly formed PS samples were dried on a hot plate at 120 °C for 10 min before the second weighing (m_2). Finally, the porosity was calculated from the weight variation, the etched area (A), the layer thickness and the silicon density ($d_{Si} = 2330$ kg·m^{-3}), as described in Eq. (1).

$$\Phi = \frac{m_1 - m_2}{A \cdot h_{PS} \cdot d_{Si}} \quad (1)$$

The sample etching conditions and the PS characteristics are summarized in Table 1. The low-porosity samples were obtained at 10 mA/cm^2 and had average porosity values between 27 ± 1% and 34 ± 1%, depending on the layer thickness. The average porosity values of the moderate-porosity samples (50 mA/cm^2) were between 40 ± 3% and 49 ± 3%, and the average porosity values of the high-porosity samples (80 mA/cm^2) were between 47 ± 3% and 62 ± 4%. It should be noted that the etching of the thickest PS layers at 50 mA/cm^2 and 80 mA/cm^2 led to local cracks in the PS layers at the edges of the PS region. Finally, PS layers with progressively decreasing porosity were investigated with the aim of improving the energy transfer between the Si and the PS by reducing the acoustic impedance mismatch at the interface between the two layers. Three PS layers with controlled porosity were synthetized, as described in a previous work [24], with layer thicknesses similar to those of the other samples. The average porosity values of the PS samples with controlled porosity were in the range of 50 ± 2% to 44 ± 2% and were the result of a gradual decrease in the local porosity with the depth (from 55% at a 25 µm depth to 35% at an 80 µm depth). The Si/PS wafers were cut into 3 × 3 cm^2 square samples. For homogeneity reasons, only the centre part of each wafer was used for the acoustic characterization. A Si sample with the same characteristics as the material used to fabricate the PS layer was also characterized as a reference to monitor the acoustic damping effect.

Table 1
Anodization parameters and resulting features of the characterized PS samples.

	Current density [mA/cm^2]	Duration [min]	Average porosity [%]	Thickness[µm]
Low porosity	10	22	27 ± 1	25.6 ± 0.2
	10	44	31 ± 1	42.1 ± 0.2
	10	88	34 ± 1	77.6 ± 0.6
Moderate porosity	50	5.75	40 ± 3	22.8 ± 0.5
	50	11.5	43 ± 2	39.4 ± 0.7
	50	23	49 ± 3	68.7 ± 1.7
High porosity	80	5	47 ± 3	25.6 ± 0.6
	80	10	54 ± 3	43.3 ± 0.8
	80	20	62 ± 4	73.1 ± 1.7
Controlled porosity	Variable	7	50 ± 2	26.6 ± 0.4
	Variable	12.5	49 ± 2	43.3 ± 0.4
	Variable	44	44 ± 2	82.1 ± 0.4

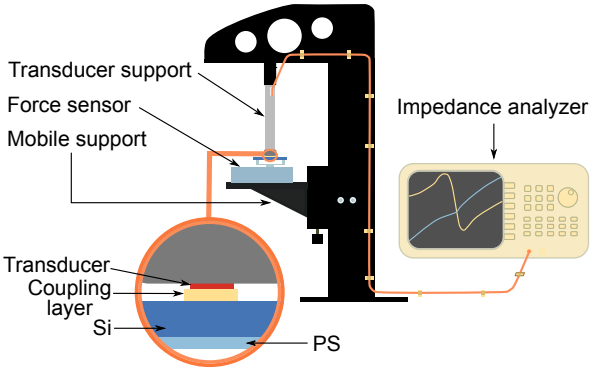

Fig. 1. Schematic representation of the experimental setup (additional information and relevant dimensions are shown in Fig. S2 in the supporting information).

2.2. Experimental protocol for acoustic characterization

The technique used for the acoustic characterization is based on the electrical impedance measurement of an ultrasonic transducer in contact with the characterized sample (i.e., the Si substrate or the Si/PS substrate). The front side of the ultrasonic transducer is then acoustically loaded by the plate under test. The experimental setup used for the in-contact measurement is presented in Fig. 1. The Si side of the plate under test was placed in contact with the transducer while the PS side was free, in contact with air, to avoid any risk of fluid infiltration into the pores. This configuration was chosen because, in the final application, the ultrasonic transducers are layered on the Si side, whereas the PS side is maintained in contact with the air. The ultrasonic transducer and the electrical cables were kept in a fixed position. The sample was placed on a mobile support to be able to contact the transducer with micrometric accuracy. A water-based acoustic gel (Aquasonic 100, Parker) was used to ensure the acoustic coupling between the transducer and the sample. A few millimetre-thick hollow plastic holder was used to hold the sample, to keep the centre of the sample rear side in contact with the air and to avoid any acoustic coupling between the holder and the sample. The sample and its holder were put onto a force sensor to control the force applied between the transducer and the sample (for additional information, see Fig. S2 in the supporting information). The use of a force sensor was necessary to ensure the repeatability and the reproducibility of the characterization method. For each measurement, the contact force was fixed at 13 N. In these conditions, the thickness of the gel layer is sufficiently thin to neglect the wave propagation in it without any risk of damage to the sample. The ultrasonic transducer was chosen in such a way that the resonance frequencies of the samples (between 8.06 MHz and 8.55 MHz for a Si thickness of 508 ± 15 µm) were in agreement within the transducer bandwidth. The measurements were carried out using a flat unfocused single-element transducer (U8436023, Olympus) with a 6 mm diameter that was centred at 10 MHz with a frequency bandwidth of 60% at −6 dB. The ultrasonic transducer was connected to an impedance analyser (HP E5100A, Agilent). The electrical impedance measurements were performed at frequencies around the resonance frequency of the substrate in a frequency range sufficiently broad to correctly measure the shift in the resonance frequency caused by the PS layer; the frequency range was also kept narrow enough to preserve the accuracy for the quality factor measurement. A frequency range of [6–10 MHz] was found to provide the best trade-off for all the samples with a pitch of 4 kHz (the smallest pitch available with our equipment).

A procedure was specifically implemented to determine the input acoustic impedance (Z_a) of the sample under test from the experimental electrical impedance curves. An ultrasonic transducer reciprocally transforms a voltage V and current I into a mechanical wave defined by a velocity v in the surrounding medium and a pressure P. As for all linear systems, the ultrasonic transducer can be modelled as a two-port electrical network defined by a 2 × 2 matrix, as described in [25]. The relationship between V, I, P and v is given by Eq. (2).

$$\begin{bmatrix} V \\ I \end{bmatrix} = \begin{bmatrix} A & B \\ C & D \end{bmatrix} \times \begin{bmatrix} P \\ v \end{bmatrix} \tag{2}$$

A and C represent two transfer functions (V/P and I/P, respectively) for the clamped acoustic boundary conditions, meaning that the incident velocity field v is null. B and D represent two transfer functions (V/v and I/v, respectively) for the free acoustic boundary conditions, meaning that the incident pressure P is null. When the transducer is loaded by a semi-infinite medium of a known characteristic acoustic impedance Z_a or a plate with an input acoustic impedance $Z_a(f)$, its electrical impedance $Z_{el}(f)$, at a given frequency of analysis f is defined by Eq. (3):

$$Z_{el}(f) = \frac{V(f)}{I(f)} = \frac{A'\cdot Z_a(f) + B'}{C'\cdot Z_a(f) + 1} \tag{3}$$

where $A' = A/D$, $B' = B/D$ and $C' = C/D$.

If A', B' and C' are known, $Z_a(f)$ is determined from the measured electrical impedance $Z_{el}(f)$, and A', B' and C' are determined from a calibration step based on the measurement of $Z_{el}(f)$ for three reference media. In this work, air ($Z_{air} \approx 0$), water ($Z_{water} = 1.5 \times 10^5$ kg·s·m^{-2}) and isopropyl alcohol ($Z_{IPA} = 0.92 \times 10^5$ kg·s·m^{-2}) [26] were chosen. For a given sample, the input acoustic impedances are thus obtained from Eq. (4).

$$Z_a(f) = \frac{Z_{el}(f) - B'}{A' - C'\cdot Z_{el}(f)} \tag{4}$$

The resonance of the plate leads to a peak (i.e., a local maximum) on the real part of the input acoustic admittance $Y_a(f) = 1/Z_a(f)$ (i.e., the acoustic conductance) at the fundamental frequency of the substrate thickness-mode resonance f_r. The resonance peak quality factor (Q) is defined from the acoustic conductance by using Eq. (5), where f_1 and f_2 are the frequencies for which the peak amplitude is divided by 2 and f_r is the resonance frequency.

$$Q = \frac{f_r}{f_2 - f_1} \qquad with \;\; f_2 > f_1 \tag{5}$$

The quality factor value of the resonance peak reflects the global acoustic damping of the Si/PS substrate; therefore, this value gives information on the acoustic attenuation in the substrate. The experimental protocol was set in such a way that the thickness of the acoustic gel layer was thin enough to be negligible and to ensure the repeatability of the contact between the transducer and the characterized sample. Using these conditions, a comparison of the quality factors of the resonance peak of the Si sample and those of the Si/PS samples can provide information on the attenuation in the PS layer. For each measurement, the quality factors were determined from the acoustic conductance at the resonance frequency. The acoustic calibration procedure was carried out before each sample characterization to avoid any drift over time in the measurements. The acoustic admittance of the Si reference sample was systematically monitored before each measurement campaign on the Si/PS samples to check the data consistency (see Fig. S3 in the supporting information).

2.3. Modelling of the input acoustic admittance of the Si/PS bilayer

The input acoustic admittance of the Si/PS plates ($Y_{Si/PS}$) was modelled by means of transmission line theory, as defined in [27]. Based on this method, the input acoustic admittance of the bilayer ($Y_{Si/PS}$) is given by Eq. (6).

$$Y_{Si/PS} = \frac{1}{Z_{Si}} \frac{Z_{Si}Y_{PS} + j\cdot\tan(k_{Si}\cdot h_{Si})}{jY_{PS}Z_{Si}\cdot\tan(k_{Si}\cdot h_{Si}) + 1} \tag{6}$$

Here, Y_{PS} is the input acoustic admittance of a stress-free PS layer defined by:

$$Y_{PS} = \frac{1}{j \cdot Z_{PS} \cdot \tan(k_{PS} \cdot h_{PS})} \tag{7}$$

Z_{Si} is the characteristic acoustic impedance of Si ($Z_{Si} = 19.7 \times 10^5$ kg·s·m^{-2} along the (1 0 0) axis [28]). k_{Si} is the longitudinal wavenumber in a Si layer with thickness h_{Si}, and k_{PS} is the longitudinal wavenumber in the PS layer with thickness h_{PS}. The acoustic losses in both materials can be considered by introducing a loss factor δ under the complex form of the wavenumber [29], as described in Eq. (8):

$$k = \frac{2 \cdot \pi \cdot f}{v \cdot (1 + j\delta)} \quad with \quad (\delta \ll 1) \tag{8}$$

where v is the longitudinal wave velocity.

The acoustic properties of the PS layer were chosen to agree with the literature. The porous frame was maintained in air; in these conditions, the longitudinal velocity in the PS layer (v_{PS}) was considered to change only with the layer porosity, as defined in Eq. (9):

$$v_{PS} = v_{Si} \cdot (1 - \Phi)^K \quad with \quad 0 < \Phi < 1 \tag{9}$$

where v_{Si} is the longitudinal velocity in Si ($v_{Si} = 8430$ m·s^{-1} along (1 0 0) axis [28]) and K is a constant that depends on the layer morphology and pore size. From [30], K was approximated according to the substrate resistivity. In our case, K was fixed at 0.8, which corresponds to a 20 mΩ·cm resistivity. Finally, the PS layer density (d_{PS}) was deduced from the layer porosity and the Si density from Eq. (10).

$$d_{PS} = d_{Si} \cdot (1 - \Phi) \quad with \quad 0 < \Phi < 1 \tag{10}$$

Two series of simulations, using the characteristics of the fabricated samples, were undertaken for PS layers with fixed porosities of 30% and 60%. The total thickness of the plate was maintained at 500 µm. The PS layer thickness was varied from 20 µm to 80 µm; therefore, the underlying Si layer thickness was reduced from 480 µm to 420 µm. Finally, the substrate resonance frequencies and peak quality factors were extracted from the simulated acoustic conductance.

3. Results and discussion

3.1. Influence of the PS layer porosity and thickness

In Fig. 2, the acoustic conductance of the moderate-porosity Si/PS samples is compared to the acoustic conductance measured on the Si reference sample (there are additional measurements provided in Fig. S4 of the supporting information). The substrate resonance peaks of the Si/PS samples are clearly distinct from those of the Si reference sample. Indeed, for all the PS layer thicknesses, the substrate resonances of the Si/PS samples are observed at higher frequencies than that of the Si reference sample. In addition, the resonance peak of the Si/PS substrates is damped compared with that of the Si substrate, even with thin layers. The characteristics of the resonance peaks were extracted for all of the samples to properly evaluate the influence of the PS layer features on the substrate resonance in comparison with the Si substrate. The resonance frequency of the Si substrate was found to be 8.09 MHz, which is in good agreement with the expected value, and the quality factor of the substrate resonance peak of the Si was equal to 190. This value is kept as a reference for the next part of the study.

The evolution of the resonance frequencies and quality factors of the Si/PS bilayer resonance peaks as a function of the PS layer thickness are represented in Figs. 3 and 4, respectively, for all the samples etched under a constant current density. In all of these cases, the Si/PS substrate resonance frequency increases with the PS layer thickness. The resonance frequency shifts from 8.31 MHz to 8.47 MHz for the low-porosity samples with thicknesses of 25.6 µm and 77.6 µm, respectively. For the highest-porosity samples, the substrate resonance ranges from

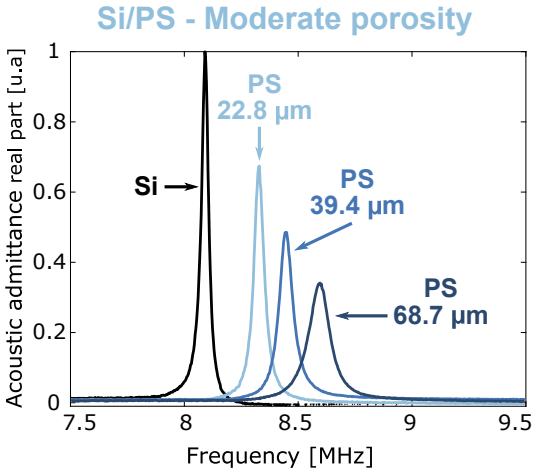

Fig. 2. Real part of the acoustic admittance of the moderate-porosity samples (blue lines) with various thickness PS layers compared to the acoustic admittance of the reference Si plate (black line). The data are normalized to the maximum value of the real part of the acoustic admittance of the Si plate. (For interpretation of the references to colour in this figure legend, the reader is referred to the web version of this article.)

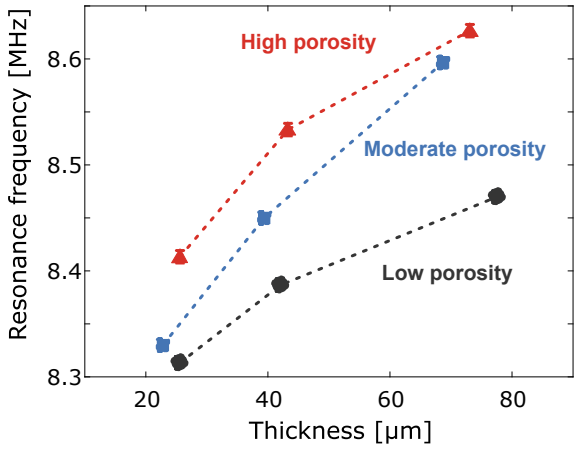

Fig. 3. Resonance frequencies extracted from the real part of the acoustic admittance of the Si/PS samples etched at constant current densities (low porosity: black circles, moderate porosity: blue squares and high porosity: red triangles) as a function of the PS layer thickness. The error bars correspond to the measurement uncertainties of 4 kHz previously estimated for the samples. The resonance frequency measured for the Si plate was 8.09 MHz. (For interpretation of the references to colour in this figure legend, the reader is referred to the web version of this article.)

8.41 MHz for the 25.6 µm thick PS to 8.63 MHz for the sample with a PS layer thickness of 73.1 µm. The quality factor is also modified by the presence of the PS layer on the rear face of the samples. The quality factor is consistently lower for the Si/PS substrates than for the Si reference plate (i.e., from 150 down to 60 for the Si/PS samples compared to 190 for the Si reference plate). These results reveal for the first time that a PS layer with a thickness much smaller than the initial wavelength in the Si has a noticeable impact on the substrate thickness-mode resonance in air. A significant decrease of 70% in the quality factor peak for the thickest and highest-porosity PS layer is obtained. As expected, the diminution of the resonance peak quality factor depends on the layer porosity. More surprisingly, these results suggest that low porosities (≈30%) are more favourable to attenuate the substrate resonance for a PS layer thickness lower than 40 µm. Indeed, a 40% peak damping is observed for the 26-µm thick low porosity sample in air.

These experimental investigations were compared to the set of

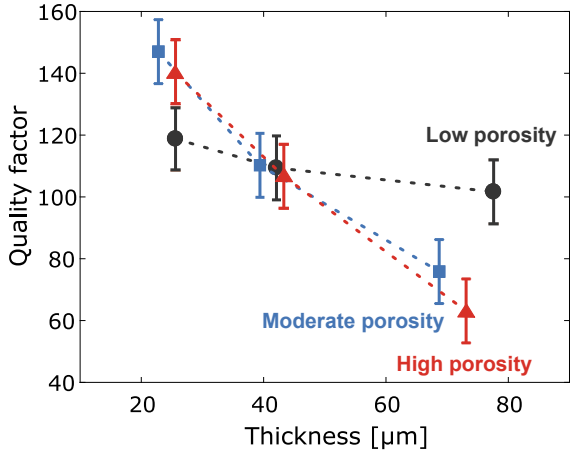

Fig. 4. Quality factors extracted from the real part of the acoustic admittance of the Si/PS samples etched at constant current densities (low porosity: black circles, moderate porosity: blue squares and high porosity: red triangles) as a function of the PS layer thickness. The error bars correspond to the measurement uncertainties of 11 previously estimated for the samples. The quality factor measured for the Si plate was 190. (For interpretation of the references to colour in this figure legend, the reader is referred to the web version of this article.)

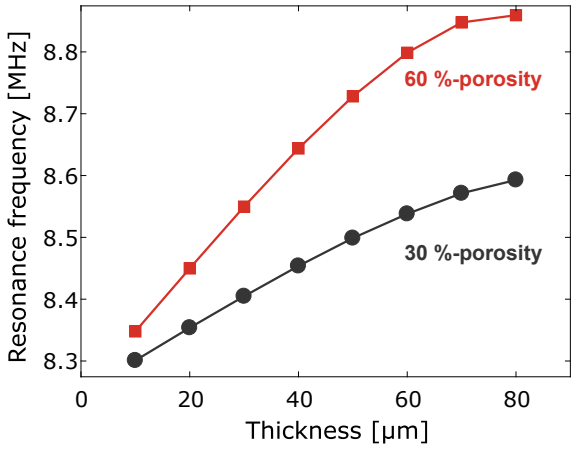

Fig. 5. Theoretical resonance frequencies extracted from the real part of the acoustic admittance simulated for the Si/PS samples (30%-porosity PS: black circles and 60%-porosity: red squares) as a function of the PS thickness.

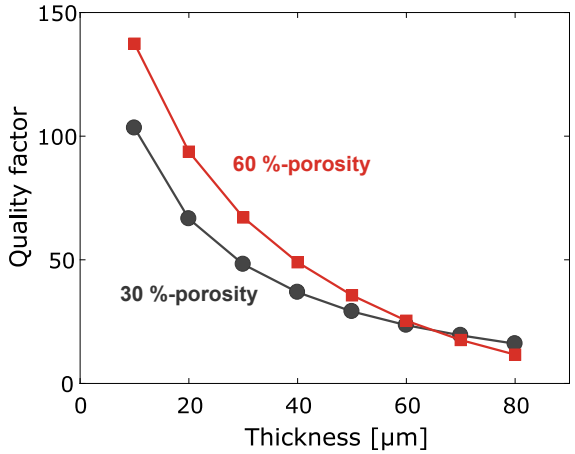

Fig. 6. Theoretical quality factor extracted from the real part of the acoustic admittance simulated for the Si/PS samples (30%-porosity PS: black circles and 60%-porosity: red squares) as a function of the PS thickness.

simulations of the Si/PS bilayer to get a better understanding of the phenomena responsible for the peak damping and the frequency shift. The losses in Si and PS were thus arbitrary fixed at $\delta_{Si} = 2.5 \cdot 10^{-3}$ and $\delta_{PS} = 3 \cdot 10^{-2}$, respectively, to be consistent with the experimental results. The resonance frequencies and the quality factors as a function of the PS layer thickness are plotted in Figs. 5 and 6, respectively, for 30% and 60% porosity values and PS layer thicknesses ranging from 20 μm to 80 μm. An increase in the PS layer thickness leads to a shift in the resonance frequency towards higher values (cf. Fig. 5), which is consistent with the experimental results. For a given PS layer thickness, the frequency shift is the highest for the highest porosity. Therefore, the quality factor decreases with an increase in the PS layer thickness; tendencies similar to those found previously are observed here. For PS layer thicknesses less than 50 μm, the most efficient way to dampen the peak is to use the lowest porosity (cf. Fig. 6). This tendency is reversed for PS layer thickness values greater than 50 μm, where the quality factor of the substrate resonance peak is smaller for the highest-porosity layers.

Considering the PS layer thickness range, the observed phenomena can be interpreted by making an analogy with the behaviour of a quartz crystal plate acoustically loaded by a thin polymer film [31–33], which dampens and decreases the resonance frequency of the Si resonator (i.e., the Si layer). The resonance frequency diminution is caused by a mass effect, and the frequency shift is proportional to the mass deposited. The resonance frequency of the Si layer is then shifted towards lower frequencies as the mass of the PS layer increases. As a consequence, for a given PS thickness, the resonance frequency of the substrate is proportional to the porosity (cf. Figs. 3 and 5). Furthermore, the Si layer thickness decreases with an increase in the PS layer thickness when the Si sample is converted into PS. Hence, the resonance frequency of the Si layer increases with the thickness of the PS layer (i.e., the resonance frequency of the Si resonator is inversely proportional to its thickness). The evolution of the resonance frequency is thus a combination of two phenomena. First, reducing the Si layer thickness increases the resonance frequency. Second, the PS layer acts as a mass and decreases the resonance frequency of the Si resonator.

A similar analysis can be performed to explain the evolution of the quality factor. As described in [33], three different regimes are observed depending on the ratio between the thin film thickness and the acoustic wavelength in the film at the resonance frequency of the substrate (h/λ). For the thinnest films ($h/\lambda < 0.05$), the quality factor is inversely proportional to the mass. Thus, for a given PS layer thickness, the damping is higher for the lowest porosity, as suggested by the experimental and theoretical results. For thicker layers ($h/\lambda < 0.1$), the damping still depends on the reverse of the mass but also highly depends on h/λ (a third-order relationship). As a result, for the same thickness, a smaller wavelength is favourable for acoustic damping. Finally, the last regime corresponds to the thin film resonance (i.e., $h = \lambda/4$), at which the maximum damping is reached. The acoustic wavelength in the PS layer is inversely proportional to the porosity; thus, when the PS layer thickness increases, the highest porosities reach the optimal $\lambda/4$-value faster than the lowest porosities. The crossing point observed in the evolution of the quality factors shown in Figs. 3 and 6 is a consequence of these phenomena. It should be noted that a thickness of $\lambda/4$ corresponds to the optimal damping; however, the acoustic damping for two PS layers with an equivalent h/λ but different porosities is not the same, since the mass must be considered. Indeed, for an equivalent h/λ, the lowest porosities are favourable for achieving a higher acoustic damping (as illustrated in Fig. S5 of the supporting data). In conclusion, for PS etched at a constant current density, thick PS layers of low porosity are more suitable to efficiently dampen the wave propagation in the substrate, and optimal damping is achieved when the layer thickness reaches the $\lambda/4$-value.

3.2. Influence of the in-depth variation in porosity

Under electrochemical etching conditions with a constant current density, the PS layer porosity monotonically increases with the depth [34] owing to HF molecule diffusion issues in the nanoscale size pores [35]. From a technological point of view, this behaviour can induce a mechanical stress or even film lift-off in the case of thick and/or high-porosity PS layers [21]. Thus, from a technological point of view, the etching of sufficiently thick layers (> 200 µm) with a low average porosity (< 30%) cannot be considered to enhance the performance of the damping layer. Consequently, it is interesting to evaluate other ways to improve the mass-loading effect. One possibility is to take advantage of the PS electrochemical etching technique to control the porosity in-depth and, thus, its in-depth acoustic properties. Hereby, we investigated PS layers with an acoustic impedance gradient (i.e., decrease in the porosity) from the layer surface towards the interface with the Si. The aim was to reduce the acoustic impedance mismatch at the interface between the two layers to improve the energy transfer between the two materials as well as to investigate the impact of the PS layer micro-structure on the acoustic damping. The resonance frequencies and quality factors extracted from the measurements of the controlled porosity samples are presented in Figs. 7 and 8, respectively, and are compared to the moderate-porosity samples (i.e., those with similar average porosity values). If only the mass-loading effect is considered, the tendencies observed for the controlled porosity samples are expected to be similar to those observed from the moderate-porosity samples, since they have comparable average porosity values (cf. Table 1). Nevertheless, the frequency shift is lower for the controlled porosity samples than for the moderate-porosity samples. Moreover, the resonance frequencies of the two thinnest controlled porosity samples are lower than those of the low-porosity samples of equivalent thicknesses (cf. Figs. 3 and 4). This first evidence indicates that the in-depth layer properties have an influence on the evolution of the quality factor. Indeed, in the investigated range of thicknesses, the quality factor of the controlled porosity samples is almost constant; the quality factor of the moderate-porosity samples decreases as the layer thickness increases. It is interesting to note that, for the thinnest layers (20 µm and 40 µm), the lowest quality factor is obtained from the controlled porosity samples; thus, the thickness of the damping layer can be reduced by adapting the acoustic impedance of the PS to that of the Si layer. Further investigations are necessary to understand the phenomena involved in such a structure. However, these results show that better performance in terms of the attenuation can be obtained by properly controlling the in-depth porosity.

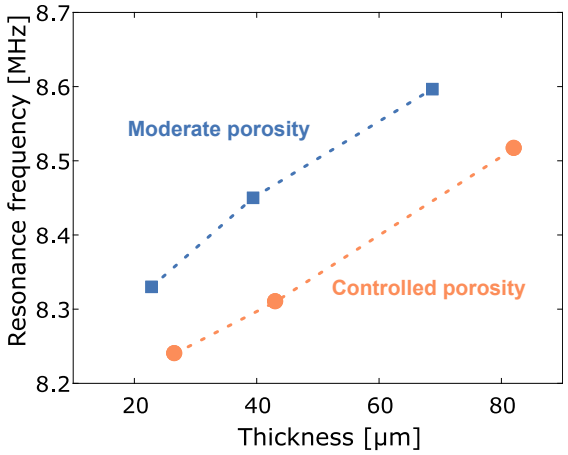

Fig. 7. Resonance frequencies extracted from the real part of the acoustic admittance of the Si/PS samples with controlled porosity (controlled porosity: orange circles) compared to the Si/PS samples of moderate porosity etched at a constant current density (moderate porosity: blue squares) as a function of the PS layer thickness. The error bars correspond here to the measurement uncertainties of 4 kHz previously estimated for the samples. The resonance frequency measured for the Si plate was 8.09 MHz. (For interpretation of the references to colour in this figure legend, the reader is referred to the web version of this article.)

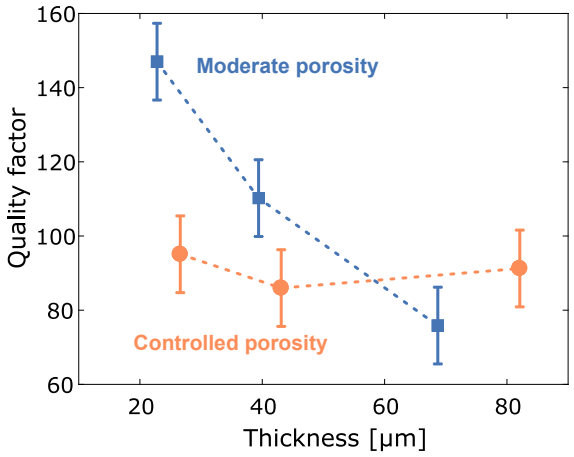

Fig. 8. Quality factors extracted from the real part of the acoustic admittance of the Si/PS samples with a controlled porosity (controlled porosity: orange circles) compared to the Si/PS samples of moderate porosity etched at a constant current density (moderate porosity: blue squares) as a function of the PS layer thickness. The error bars correspond to the measurement uncertainties of 11 previously estimated for the samples. The quality factor measured for the Si plate was 190. (For interpretation of the references to colour in this figure legend, the reader is referred to the web version of this article.)

4. Conclusions

Several sets of silicon/porous silicon substrates were fabricated. Their resonance frequencies and the attenuation of their thickness-mode resonance values were measured in a relevant ultrasound imaging range of frequencies (from 6 to 10 MHz). The results indicate that porous silicon layers are suitable for optimizing the axial resolution of ultrasonic transducers integrated on a silicon substrate. More specifically, this optimization can be achieved by a proper combination of the layer porosity and thickness. In the samples tested, the most efficient combination was a porosity of 62% and a thickness of 73 µm, which achieved a damping of 70% of the substrate resonance. A descriptive model based on transmission line theory was used to define the general rules for the design of optimal built-in porous silicon acoustic dampers. The most effective way to dampen the substrate resonance is to reduce the porosity and increase the layer thickness (i.e., to close to a quarter of the wavelength in the porous silicon). Finally, by progressively decreasing the porosity of the layer to adapt the acoustic impedance from the silicon towards the porous silicon, the thickness of the porous silicon layer can be reduced to 27 µm. To the best of our knowledge, this study is the first to show evidence of the efficacy of silicon/porous silicon substrates dampening the substrate resonance to improve the axial resolution of ultrasonic transducers. The design rules reported in this article are also applicable to other thin attenuating layers suitable for integration with the ultrasound-based micro-systems in development to overcome the next challenges of ultrasound imaging (e.g., high-frequency transducers, flexible devices, and *in vivo* imaging). Future investigations should focus on clarifying how the porous silicon morphology (i.e., the pore diameter and shape) and the evolution of in-depth porosity influence the substrate damping. The final goal of this work is to integrate an ultrasonic transducer on a silicon substrate with a built-in porous silicon acoustic damping layer to evaluate its impulse response (i.e., the pulse duration and bandwidth) and the potential benefit to the axial resolution of ultrasound images.

Acknowledgement

This work was supported by the “Région Centre” in the framework of the SIPeMUT research project [2013-00083160] and the “Conseil Départemental d’Indre et Loire”.

Appendix A. Supplementary material

Supplementary data to this article can be found online at https://doi.org/10.1016/j.ultras.2019.01.006.

References

[1] C. Tekes, G. Gurun, M.W. Rashid, J. Zahorian, T. Xu, J. Hasler, F.L. Degertekin, 3-D real-time volumetric imaging using 20 MHz 1.5-mm diameter single-chip CMUT-on-CMOS array, Ultrason. Symp. IUS 2012 IEEE Int. IEEE, 2012, pp. 1–4, , https://doi.org/10.1109/ULTSYM.2012.0514.

[2] F.L. Degertekin, R.O. Guldiken, M. Karaman, Annular-ring CMUT arrays for forward-looking IVUS: transducer characterization and imaging, IEEE Trans. Ultrason. Ferroelectr. Freq. Contr. 53 (2006) 474–482, https://doi.org/10.1109/TUFFC.2006.1593387.

[3] C. Dagdeviren, Y. Su, P. Joe, R. Yona, Y. Liu, Y.-S. Kim, Y. Huang, A.R. Damadoran, J. Xia, L.W. Martin, Y. Huang, J.A. Rogers, Conformable amplified lead zirconate titanate sensors with enhanced piezoelectric response for cutaneous pressure monitoring, Nat. Commun. 5 (2014), https://doi.org/10.1038/ncomms5496.

[4] C. Wang, X. Li, H. Hu, L. Zhang, Z. Huang, M. Lin, Z. Zhang, Z. Yin, B. Huang, H. Gong, S. Bhaskaran, Y. Gu, M. Makihata, Y. Guo, Y. Lei, Y. Chen, C. Wang, Y. Li, T. Zhang, Z. Chen, A.P. Pisano, L. Zhang, Q. Zhou, S. Xu, Monitoring of the central blood pressure waveform via a conformal ultrasonic device, Nat. Biomed. Eng. 2 (2018) 687–695, https://doi.org/10.1038/s41551-018-0287-x.

[5] P.C. Eccardt, K. Niederer, B. Fischer, Micromachined transducers for ultrasound applications, 1997 IEEE Ultrason. Symp. Proc. Int. Symp. Cat No97CH36118, IEEE, Toronto, Ont., Canada, 1997, pp. 1609–1618, , https://doi.org/10.1109/ULTSYM.1997.663304.

[6] Matthew I. Haller, Butrus T. Khuri-Yakub, A surface micromachined electrostatic ultrasonic air transducer, Proc. IEEE Ultrason. Symp. ULTSYM-94, vol. 2, IEEE, Cannes, France, 1994, pp. 1241–1244, , https://doi.org/10.1109/ULTSYM.1994.401810.

[7] I.O. Wygant, Xuefeng Zhuang, D.T. Yeh, O. Oralkan, A.S. Ergun, M. Karaman, B.T. Khuri-Yakub, Integration of 2D CMUT arrays with front-end electronics for volumetric ultrasound imaging, IEEE Trans. Ultrason. Ferroelectr. Freq. Control. 55 (2008) 327–342, https://doi.org/10.1109/TUFFC.2008.652.

[8] I. Ladabaum, P. Wagner, C. Zanelli, J. Mould, P. Reynolds, G. Wojcik, Silicon substrate ringing in microfabricated ultrasonic transducers, Ultrason. Symp. 2000 IEEE, IEEE, 2000, pp. 943–946, , https://doi.org/10.1109/ULTSYM.2000.922696.

[9] X. Jin, O. Oralkan, F.L. Degertekin, B.T. Khuri-Yakub, Characterization of one-dimensional capacitive micromachined ultrasonic immersion transducer arrays, IEEE Trans. Ultrason. Ferroelectr. Freq. Contr. 48 (2001) 750–760, https://doi.org/10.1109/58.920706.

[10] I. Ladabaum, P.A. Wagner, Microfabricated Acoustic Transducer with Suppressed Substrate Modes, US6862254B2, 2005.

[11] V. Lehmann, Electrochemical pore formation, Electrochem. Silicon, Wiley-VCH Verlag GmbH, Weinheim, FRG, 2002, pp. 97–126, , https://doi.org/10.1002/3527600272.

[12] G. Gautier, T. Defforge, S. Desplobain, J. Billoué, M. Capelle, P. Povéda, K. Vanga, B. Lu, B. Bardet, J. Lascaud, C. Seck, A. Fèvre, S. Menard, L. Ventura, Porous silicon in microelectronics: from academic studies to industry, ECS Trans. 69 (2015) 123–134, https://doi.org/10.1149/06902.0123ecst.

[13] X. Zhang, Morphology and formation mechanisms of porous silicon, J. Electrochem. Soc. 151 (2004) C69, https://doi.org/10.1149/1.1632477.

[14] A. Loni, Porous silicon formation by anodization, Handb. Porous Silicon, Springer, Cham, 2014, pp. 11–22, , https://doi.org/10.1007/978-3-319-05744-6_2.

[15] P. Hasan, V. Sajith, M.S. Ansari, J. Iqbal, A. Alshahrie, Influence of HF concentration and current density on characteristic morphological features of mesoporous silicon, Micropor. Mesopor. Mater. 249 (2017) 176–190, https://doi.org/10.1016/j.micromeso.2017.04.059.

[16] E.C. Wu, J.S. Andrew, L. Cheng, W.R. Freeman, L. Pearson, M.J. Sailor, Real-time monitoring of sustained drug release using the optical properties of porous silicon photonic crystal particles, Biomaterials 32 (2011) 1957–1966, https://doi.org/10.1016/j.biomaterials.2010.11.013.

[17] G.N. Aliev, B. Goller, P.A. Snow, H. Heinrich, B. Yuan, R. Aigner, Porous silicon bulk acoustic wave resonator with integrated transducer, Nanosc. Res. Lett. 7 (2012) 378, https://doi.org/10.1186/1556-276X-7-378.

[18] R. Da Fonseca, J. Saurel, A. Foucaran, E. Massone, T. Taliercio, J. Camassel, Acoustic microscopy investigation of porous silicon, Thin Solid Films 255 (1995) 155–158, https://doi.org/10.1016/0040-6090(94)05643-R.

[19] L. Canham, Mechanical properties of porous silicon, Handb. Porous Silicon, Springer, Cham, 2014, pp. 213–220, , https://doi.org/10.1007/978-3-319-05744-6_21.

[20] F. Hamdi, S. Bouhedja, H. Amrani, Theoretical study of different attenuation measurement by acoustic microscopy, J. Appl. Phys. 114 (2013) 133501, https://doi.org/10.1063/1.4823850.

[21] M. Capelle, J. Billoué, T. Defforge, P. Poveda, G. Gautier, Evaluation of mesoporous silicon substrates strain for the integration of radio frequency circuits, Thin Solid Films 585 (2015) 66–71, https://doi.org/10.1016/j.tsf.2015.04.022.

[22] D. Brumhead, L. Canham, D. Seekings, P. Tufton, Gravimetric analysis of pore nucleation and propagation in anodised silicon, Electrochim. Acta 38 (1993) 191–197, https://doi.org/10.1016/0013-4686(93)85128-L.

[23] Characterization of Porous Silicon, in: Porous Silicon Pract., Wiley-VCH Verlag GmbH & Co. KGaA, 2012, pp. 133–187. https://doi.org/10.1002/9783527641901.ch5.

[24] J. Lascaud, T. Defforge, D. Certon, D. Valente, G. Gautier, In-depth porosity control of mesoporous silicon layers by an anodization current adjustment, J. Appl. Phys. 122 (2017) 214903, https://doi.org/10.1063/1.4997228.

[25] A.L. Lopez-sanchez, L.W. Schmerr, Determination of an ultrasonic transducer’s sensitivity and impedance in a pulse-echo setup, IEEE Trans. Ultrason. Ferroelectr. Freq. Contr. 53 (2006) 2101–2112, https://doi.org/10.1109/TUFFC.2006.150.

[26] A.R. Selfridge, Approximate material properties in isotropic materials, IEEE Trans. Son. Ultrason. 32 (1985) 381–394, https://doi.org/10.1109/T-SU.1985.31608.

[27] V.E. Granstaff, S.J. Martin, Characterization of a thickness-shear mode quartz resonator with multiple nonpiezoelectric layers, J. Appl. Phys. 75 (1994) 1319–1329, https://doi.org/10.1063/1.356410.

[28] D. Royer, E. Dieulesaint, Elastic Waves in Solids I: Free and Guided Propagation, Springer-Verlag, Berlin Heidelberg, 2000, p. 177.

[29] J.D.N. Cheeke, Acoustic waveguides, Fundam. Appl. Ultrason. Waves, second ed., CRC Press, 2017, pp. 151–172.

[30] G.N. Aliev, B. Goller, P.A. Snow, Elastic properties of porous silicon studied by acoustic transmission spectroscopy, J. Appl. Phys. 110 (2011) 043534, https://doi.org/10.1063/1.3626790.

[31] X. Qiao, X. Zhang, Y. Tian, Y. Meng, Progresses on the theory and application of quartz crystal microbalance, Appl. Phys. Rev. 3 (2016) 031106, https://doi.org/10.1063/1.4963312.

[32] R. Lucklum, P. Hauptmann, The quartz crystal microbalance: mass sensitivity, viscoelasticity and acoustic amplification, Sens. Actuat. B Chem. 70 (2000) 30–36, https://doi.org/10.1016/S0925-4005(00)00550-5.

[33] D. Johannsmann, Stratified layer systems, Quartz Cryst. Microbalance Soft Matter Res. Springer, Cham, 2015, pp. 221–246, , https://doi.org/10.1007/978-3-319-07836-6_10.

[34] S. Foss, P. Kan, T. Finstad, Single beam determination of porosity and etch rate in situ during etching of porous silicon, 114909–114909, J. Appl. Phys. 97 (2005), https://doi.org/10.1063/1.1925762.

[35] V. Lehmann, The physics of macropore formation in low doped n-type silicon, J. Electrochem. Soc. 140 (1993) 2836, https://doi.org/10.1149/1.2220919.